JOURNAL OF MATERIALS SCIENCE **40** (2005) 5207–5214

Microstructure and microwave properties of $CaTiO_3$–$LaGaO_3$ solid solutions

H. ZHENG*, GDC CSETE DE GYÖRGYFALVA, I. M. REANEY
Department of Engineering Materials, University of Sheffield, Sheffield, S1 3JD, UK
E-mail: h.zheng@sheffield.ac.uk

The phase assemblage, microstructure and microwave (MW) properties of xCaTiO$_3$-$(1-x)$LaGaO$_3$ (CT-LG) ceramics prepared by solid state synthesis from raw oxides and carbonates have been investigated. LG was predominantly single phase perovskite with space group, *Pnma*, but a small quantity of pyrochlore structured $La_2Zr_2O_7$ second phase was present due to the contamination from the ZrO_2 milling media. At MW frequencies, the temperature coefficient of resonant frequency (τ_f) of LG was –80 ppm/°C, its permittivity, $\varepsilon_r = 27$ and MW quality factor, $Q^* f_o = 97{,}000$ (@5 GHz). As CT concentration increased, τ_f and ε_r increased to +850 ppm/°C and 160, respectively but $Q^* f_o$ decreased to ~20,000. Zero τ_f was achieved at $x \approx 0.65$ with $\varepsilon_r \approx 47$, and $Q^* f_o \approx 40{,}000$, properties comparable with commercial compositions. However, for $x = 0.5$, a different second phase was observed which was rich in Ca and Ga. Electron diffraction patterns could be indexed according to a body centred cubic lattice, $a \approx 12.5$ Å. It is suggested that the presence of second phases in the CT-LG compounds may, in part, be responsible for the deterioration in $Q^* f_o$.

1. Introduction

$CaTiO_3$-based perovskite ceramics are widely used as resonator materials in wireless communication systems. These applications require a combination of high relative permittivity (ε_r), high quality factor ($Q^* f_o$) and near-zero temperature coefficient of the resonant frequency (τ_f). $CaTiO_3$ (CT) exhibits a high relative permittivity of 160, which is however accompanied by a large positive τ_f value of 850 ppm/°C [1]. In contrast, other simple perovskites such as $NdAlO_3$ (NA) [2] and $LaGaO_3$ (LG) [3] have moderate permittivities of 20–30 combined with small negative τ_f values. Thus, potentially useful ceramics with temperature stable and relative permittivities of 40–50 can be obtained by forming solid solutions between CT and NA or LG. CT-NA solid solutions have been intensively investigated and the zero-τ_f CT-NA composition with $Q^* f_o > 40000$ GHz has been developed and first patented by Kyocera, Japan in 90 s. Recently high $Q^* f_o$ (>40000 GHz) values have also been reported for zero-τ_f CT-LG compounds [3]. However, due to difficulties in preparing high-purity, single-phase CT-LG compounds via high-temperature solid state sintering, studies on the CT-LG solid solutions have been scarce. CT and LG have the same space group and Glazer tilt system at room temperature ($a^-a^-c^+$, *Pnma*) [4, 5] and a solid solution between the two compounds will retain the same structure. Consequently, the effect of composition on MW dielectric properties may be considered without the complication of a change in crystal class due to the onset structural phase transitions.

The purpose of the present work is to investigate the phase assemblage, microstructures of xCaTiO$_3$-$(1-x)$LaGaO$_3$ (CT-LG) solid solutions, using X-ray diffraction (XRD), scanning (SEM), and

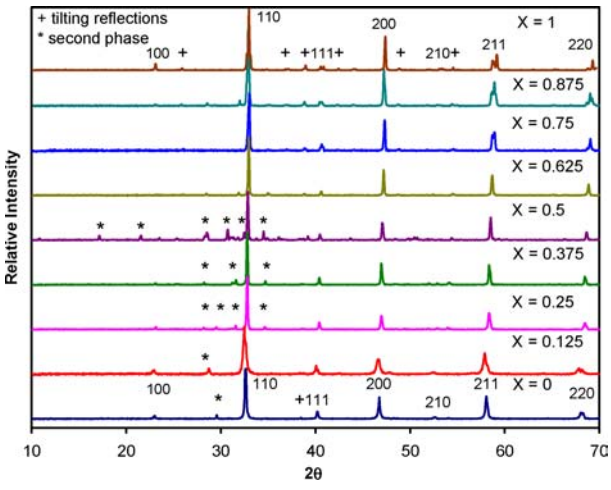

Figure 1 XRD traces from the sintered ceramics of xCaTiO$_3$-$(1-x)$LaGaO$_3$ (CT-LG) solid solutions where $x = 0$, 0.125, 0.25, 0.375, 0.5, 0.625, 0.75, 0.875 and 1. '+' indicates superlattice reflections arising from distortion of the perovskite lattice. '∗' indicates second phase peaks.

*Author to whom all correspondence should be addressed.
0022–2461
DOI: 10.1007/s10853-005-4414-1

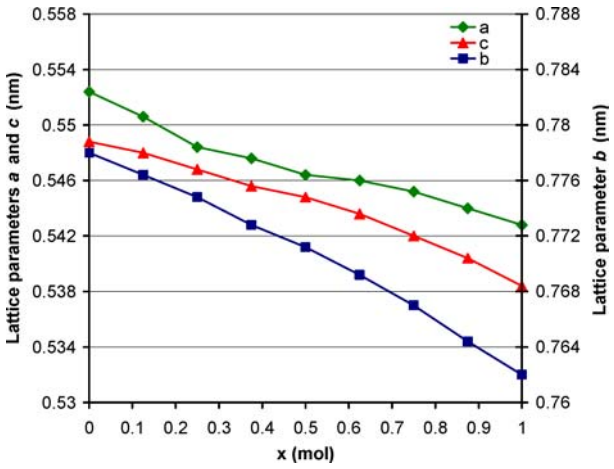

Figure 2 Lattice parameters a, b, c as a function of x in CT-LG ceramics.

transmission (TEM) electron microscopy equipped with energy-dispersive-spectroscopy (EDS). The effect of the presence of second phases on dielectric properties of the CTLG ceramics is also addressed.

2. Experimental

Ceramics were synthesised by a conventional mixed oxide route using $CaCO_3$, TiO_2, La_2O_3 and Ga_2O_3. The chemical purity of all these raw starting materials was >99%. The weighed starting reagents in appropriate ratios were milled (∼1 μm mean particle size, Laser Coulter Analyser) in propan-2-ol in a high-energy attrition mill (Szegvari Attritor System, Union Process, Ohio, USA) for 2 h, using zirconia media. The slurry was dried, sieved and then calcined 4–6 h at temperatures between 1300 to 1550°C, depending on composition. Calcined powder was re-milled, sieved and then pressed into discs. Discs were sintered 4 h on zirconia boards at temperatures between 1500 and 1650°C. All the fired samples have relative densities above 96%.

An X-ray diffractometer (Model PW 1730/10 Philips, Holland) with Cu K_α source ($\lambda = 1.540562$ Å), operated at 50 kV and 30 mA, was used for the identification of phases. A step size of 0.02°, a scan rate of 1°/min, and scan ranges of 10–70° were adopted.

Polished ceramics for SEM were thermally etched 100°C below their sintering temperature for 30 min

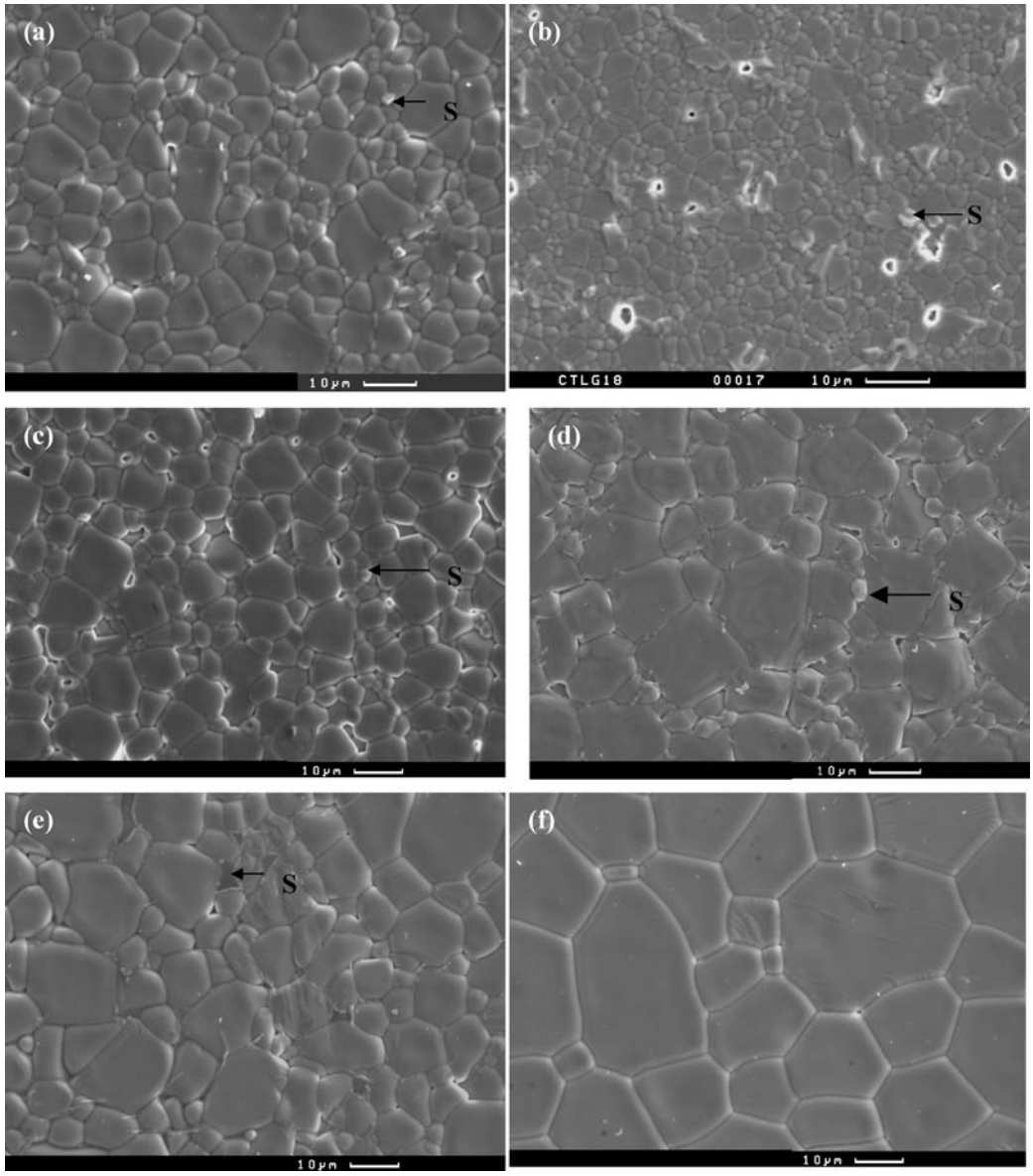

Figure 3 (3a–f) Secondary electron SEM images of CT-LG ceramics where $x = 0$, 0.125, 0.25, 0.5, 0.625 and 0.875, respectively. **S** indicates region of second phase.

and then coated with carbon before SEM examination. A CAMSCAN SEM (Series II, Cambridge, England), operating at 20 kV was used to image the grain structures of the samples. For TEM, pieces, approximately 3 mm diameter, were mounted on a Gatan disc grinder stub using Crystalbond 'heat on/heat off' resin. The ceramic was ground flat on one side using the Gatan disc grinder, removed from the Gatan disc grinder stub and remounted with the flat side down. The sample was further ground to approximately 20 μm thick and a 3.05 mm Cu support ring with 800 μm circular hole was glued onto its surface using an epoxy resin. The sample was removed from the stub and excess Crystalbond cleaned off its surface using acetone. The samples were thinned in a Gatan Duo Mill ion beam thinner operating at an accelerating voltage of 6 kV and a combined gun current of 0.6 mA at an incidence angle of 15°. The samples were examined using a Philips Tecnai TEM equipped with EDS, operating at an accelerating voltage of 200 kV.

Microwave measurements (ε_r, Q and τ_f) were performed using a silver plated aluminium cavity $>\sim 4$ times the diameter of the test resonator (this ensured an "isolated" but shielded resonator) and an Agilent vector network analyser (8753ES) with a range from 30 kHz–6 GHz. Sintered samples were located at the centre of the cavity on a 99.5% alumina support, thus avoiding any influence from the metallic cavity walls. Microwave energy was coupled to the test piece using a single probe, measuring in reflectance. After calibration for the cables and cavity, the coupling was adjusted such that losses were lower than -30 dB. Q is approximated using Equation 1,

$$Q = f_0/BW \tag{1}$$

where f_o is the resonant frequency and BW is the bandwidth measured at 7 dB from the resonant peak minimum. Measurement of Q was at ambient temperature and the resonance mode measured was $TE_{01\delta}$. τ_f measurements were performed in the same aluminium cavity placed inside a Tenney temperature control cabinet. Resonant frequency measurements were performed at 60, 20 and -10°C when the $TE_{01\delta}$ mode was stable. τ_f was calculated using Equation 2,

$$\tau_f = (f_{60} - f_{-10})/(f_{20} \times 70) \tag{2}$$

where f_{60} is the resonant frequency at 60°C, f_{-10} is the resonant frequency at -10°C and f_{20} is the resonant frequency at 20°C.

3. Results and discussion

3.1. XRD

Fig. 1 shows the XRD traces from the sintered ceramics of $x CaTiO_3$-$(1-x)LaGaO_3$ (CT-LG) solid solutions where $x = 0, 0.125, 0.25, 0.375, 0.5, 0.675, 0.75, 0.875$, and 1. All the major peaks are indexed according to a pseudocubic (p) unit cell but minor peaks are present in traces where $x \leq 0.5$. Reflections marked as "+" are arise from structural distortions of the perovskitre lattice due to rotations of the oxygen octahedral [4] but the peaks marked as "*" are the reflections associated with the presence of second phases. The room-temperature structure of $CaTiO_3$ can be described by orthorhombic symmetry, space group *Pnma*, resulting from an $a^-a^-c^+$ tilt system [4] and the XRD pattern may be indexed according to ICDD card: 42-423. At room

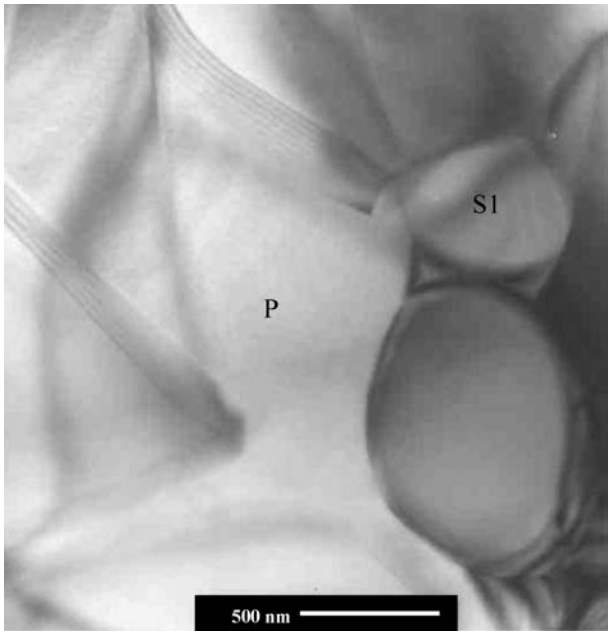

Figure 4 Bright-field (BF) TEM image of a typical region of LG ($x = 0$) showing the matrix and second phase (**S1**).

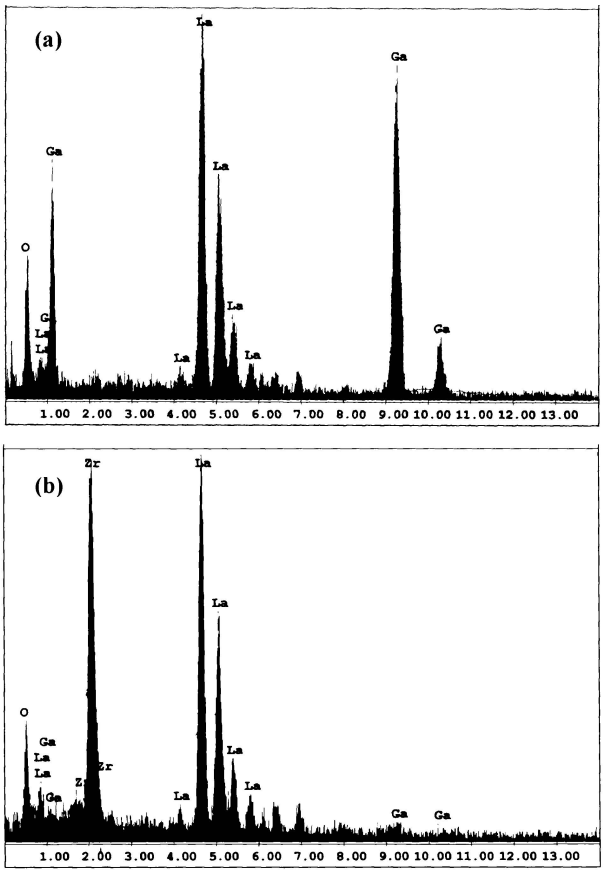

Figure 5 EDS traces from (a) the LG matrix and (b) second phase (**S1**).

temperature, LG also has the orthorhombic structure with space group, *Pnma* [5], isostructual with CT.

With increasing x, lattice parameters a, b, and c change almost linearly from LG to CT, Fig. 2, indicating the formation of solid solutions. Although the perovskite phase dominates throughout the solid solution series, second phases are also detected (denoted by "*" in Fig. 1). In LG, $La_2Zr_2O_7$ has been tentatively identified with the 100% peak visible at $\sim 29^\circ$ (2θ) and its presence is believed to arise from the contamination by ZrO_2 milling media. In general, the relative intensities of the second phase peaks increase with x until $x = 0.5$, above which they are either absent or below the detection limit of the diffractometer. Moreover, the positions of the XRD peaks associated with the second phases vary with x, suggesting that there may be more than one type present. The low relative intensity of the second phase prohibits their unambiguous identification using only XRD and further characterisation techniques are required to understand the phase assemblage in CT-LG.

3.2. SEM

Fig. 3a–f are SEM images of CT-LG ceramics where $x = 0$, 0.125, 0.25, 0.5, 0.625 and 0.875, respectively. Little porosity is observed across the whole series, consistent with measured densities >95% of the theoretical X-ray density. The grain size was monomodal in each sample and generally increased with x from ~ 5 μm in LG to ~ 10 μm in CT-LG, $x = 0.875$. The exception to this trend was $x = 0.125$, which exhibited the smallest grain size (~ 2 μm). In addition to the matrix grains in LG ($x = 0$) second phase appears as small, bright grains, arrowed in Fig. 3a. Further analysis using EDS revealed that these second phase grains were

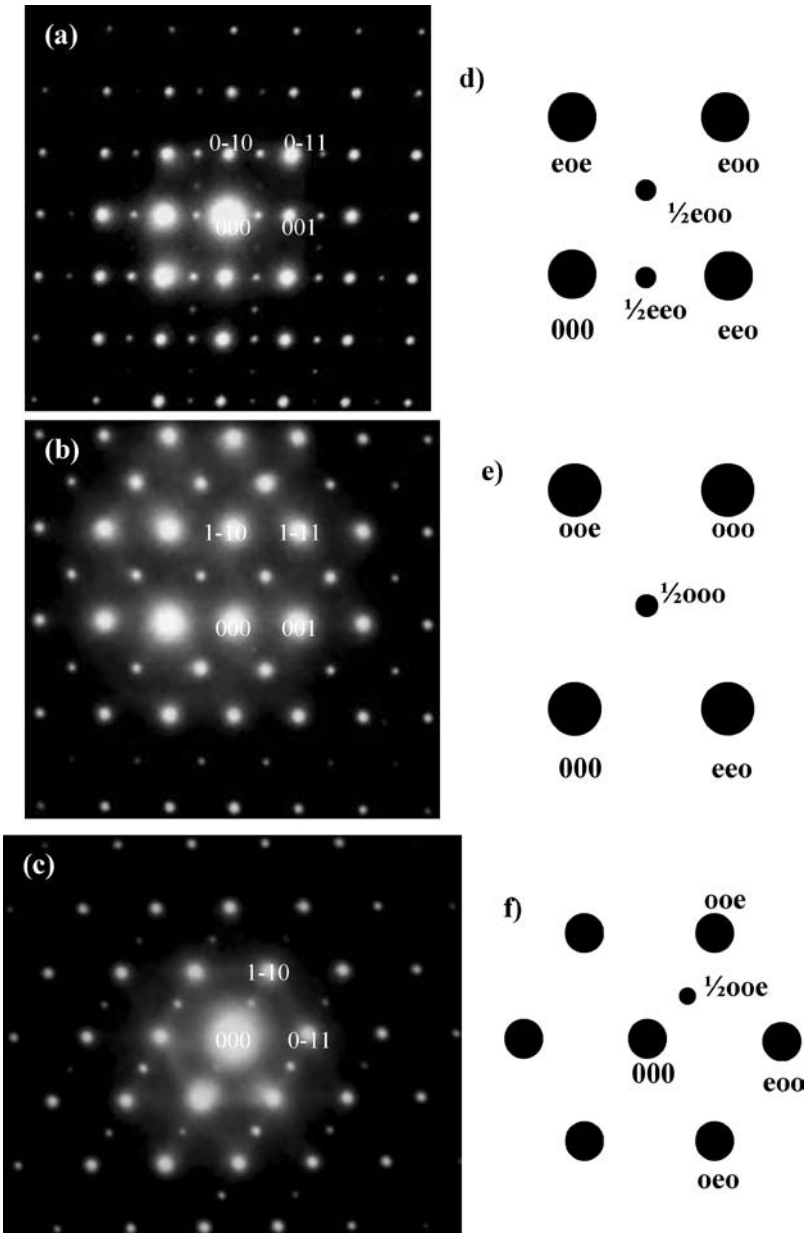

Figure 6 (a–c) $\langle 100 \rangle_p$, $\langle 110 \rangle_p$ and $\langle 111 \rangle_p$ zone axis electron diffraction patterns (ZADP's), respectively, from the perovskite structured matrix phase. Accompanying each pattern is schematic illustrating the position of $\frac{1}{2}\{ooo\}$ $\frac{1}{2}\{ooe\}$ and $\frac{1}{2}\{oee\}$ reflections associated with antiphase and in phase rotation of the octahedra and antiparallel A-site cation displacements, respectively.

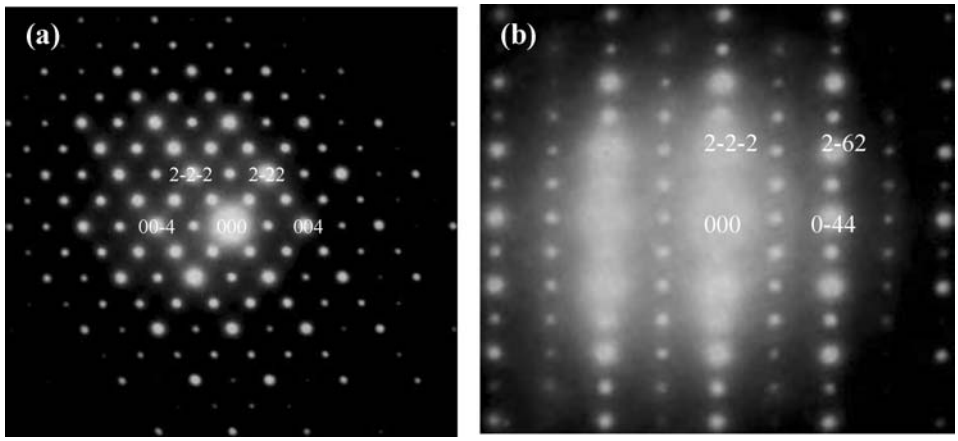

Figure 7 (a and b) ⟨110⟩ and ⟨211⟩ ZADP's, respectively, from the pyrochlore structured $La_2Zr_2O_7$ second phase (**S1**) in Fig. 4.

rich in La, Zr, O but that Ca, Ga, and Ti were also present. However, this analysis was considered inaccurate due to the large interaction volume used to obtain the EDS trace in SEM. Instead the higher spatial resolution obtained using EDS within the TEM will be used to determine the approximate chemical composition of the second phase. Bright grains of second phase were also observed in $x = 0.125$, 0.375 and 0.5 (Fig. 3b–d, respectively) whereas in $x = 0.625$ the second phase exhibited dark contrast and $x = 0.875$ appeared single phase. EDS analysis using TEM rather than SEM will be used to identify these phases.

3.3. TEM

Fig. 4 is the bright-field (BF) TEM image, of a typical region of LG ($x = 0$). The image contains a matrix phase (**P**), which exhibits planar defects typical of ferroelastic domain boundaries and a second phase grain (**S1**). EDS data indicate that the composition of the matrix grain is approximately equivalent to the nominal batched composition ($LaGaO_3$), Fig. 5a, but the second phase particle contains only La, Zr cations in approximately a 50:50 ratio, Fig. 5b.

Three zone axis electron diffraction patterns (ZADP's) from the matrix phase are shown in Fig. 6a–c. The strongest reflections may be attributed to a simple perovskite structure and therefore the patterns have been indexed as $\langle 100 \rangle_p$, $\langle 110 \rangle_p$ and $\langle 111 \rangle_p$ zone axes, respectively (where $p =$ pseudocubic). However, weaker superlattice reflections are observed at $^1/_2\{ooo\}$, $^1/_2\{ooe\}$ and $^1/_2\{oee\}$ positions as indicated in the schematics adjacent to each pattern. $LaGaO_3$ is ascribed a *Pnma* space group [5] in the ICDD data files which arises from an $a^-a^-c^+$according to the Glazer [4] notation. The $a^-a^-c^+$ tilt system describes a structure in which the octahedra around one of the orthogonal axes are tilted in phase ('+' superscript) and the other two in anti-phase but with equal magnitude ('−' superscript). In addition, the structure is further complicated by a displacement of A-site cations in antiparallel along $\langle 110 \rangle_p$ directions. According to Glazer [6], the superlattice reflections associated with antiphase and in phase tilting and antiparallel displacements occur at $\frac{1}{2}\{ooo\}$ where

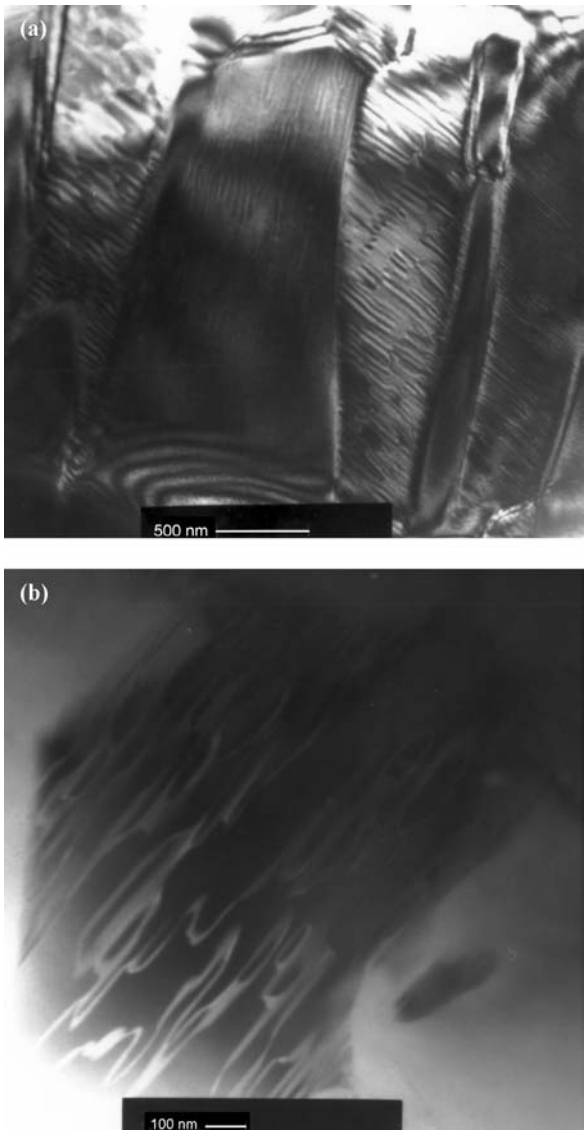

Figure 8 (a and b). BF TEM images from CTLG, $x = 0.5$ grains, showing ferroelastic twin domains and antiphase boundaries (APB's) typical of a perovskite phase distorted due to rotations of oxygen octahedra.

$h \neq k$, $\frac{1}{2}\{ooe\}$ where $h \neq k$ and $\frac{1}{2}\{oee\}$ positions, respectively. However if double diffraction is taken into account, then the superlattice reflections such as $\frac{1}{2}\{ooo\}$ where $h = k$, and $\frac{1}{2}\{ooe\}$ where $h = k$ may also appear.

Reaney *et al.* [7] have suggested that these reflections may occur by the generic double diffraction route,

$$\frac{1}{2}\{311\} + \frac{1}{2}\{\bar{2}00\} \rightarrow \frac{1}{2}\{111\}.$$

It is therefore confirmed that all the superlattice reflections in Fig. 6a–c are consistent with the $a^-a^-c^+$ tilt system of the LG structure.

In contrast, the ZADP's from the second phase particles, Figs. 7a–b, are distinctively different from those of the perovskite grains and may be indexed according to the $\langle 110 \rangle$ and $\langle 211 \rangle$ zone axes of a face centred cubic structure ($a \approx 10.7$ Å). However, due to the dynamical nature of electron diffraction it is difficult to ascribe a space group based on systematic absences. $La_2Zr_2O_7$ has the pyrochlore structure which is face centred cubic with $a = 10.8$ Å and space group *Fd3m* (ICDD card 73-444). In electron diffraction, reflections forbidden by the diamond glide (d) such as (002) and (2-20) in the *Fd3m* space group may appear due to double diffraction via routes:

$$(\text{-}111) + (1\text{-}11) = (002)$$
$$(1\text{-}1\text{-}1) + (1\text{-}11) = (2\text{-}20)$$

The experimental diffraction patterns are therefore consistent with the presence of $La_2Zr_2O_7$ but are insufficient to unambiguously identify the second phase. However, if the XRD peaks (Fig. 1) and the EDS data (Fig. 5b) are taken into account, the compound is confirmed as $La_2Zr_2O_7$.

Fig. 8a is a BF TEM image of a grain in CTLG $x = 0.5$, showing ferroelastic twin domains consistent with the presence of a distorted perovskite-structured matrix. Similar domains were observed throughout the solid solution series. In addition, planar defects with ribbon-like contrast typical of anti-phase boundaries can also be observed, Fig. 8b that were also present throughout the solid solution particularly for $x > 0.125$. APB's typically arise in simple perovskites by the impingement of regions of either octahedral rotations or antiparallel cation displacements, which have nucleated out of phase [7]. Electron diffraction patterns from the perovskite matrix in CT-LG, $x = 0.5$ are identical to those of LG shown in Fig. 6 and are therefore consistent with the $a^-a^-c^+$ tilt system and *Pnma* space group, present at room temperature throughout the solid solution.

Fig. 9a shows a triple-junction in CTLG $x = 0.5$, containing a second phase grain (**S2**). Fig. 9b–c are the

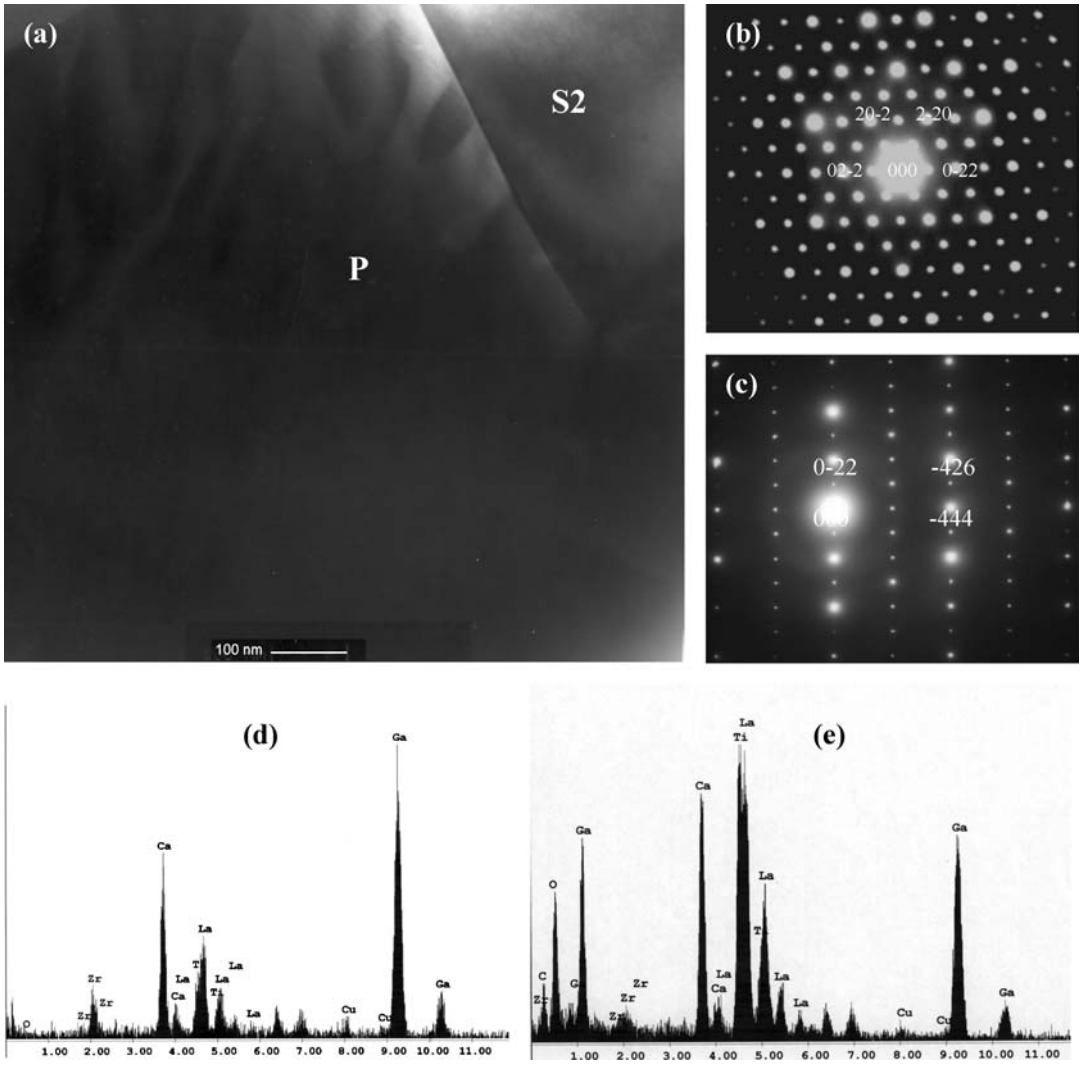

Figure 9 (a) triple-junction in CTLG, $x = 0.5$ containing a second phase grain (**S2**), (b) and (c) $\langle 111 \rangle$ and (c) $\langle 211 \rangle$ ZADP's respectively from the second phase grain indexed according to a body centred cubic structure ($a \approx$ 12.5 Å). (d) and (e) EDS spectra from the second phase (**S2**) and the perovskite-structured (**P**) grains.

ZADP's from the second phase grain, which may be indexed according to the ⟨111⟩ and ⟨211⟨ zone axes of a body centred cubic structure ($a \approx 12.5$ Å). Figs 9d–e are the EDS spectra from the perovskite and second phase grains, respectively. The spectrum from the perovskite grain is consistent with the approximate batched composition (0.5CT-0.5LG) whereas the second phase is rich in Ca, Ga, Zr and deficient in La, and Ti with respect to the matrix. Crystallographic data corresponding to a compound with a similar composition to that observed in this study has not been reported. However it is believed that the structure of this second phase is similar to that of $La_3Sc_2Ga_3O_{12}$ (body-centred cubic $a = 12.847$ Å, ICDD card 27-228), a compound with general formula $A_3B_5O_{12}$.

3.4. Dielectric properties

Fig. 10 is a plot of the measured relative permittivity ε_r and τ_f as a function of x for the CT-LG series. τ_f and ε_r increase with x and are almost linearly proportional to each other as illustrated in Fig. 11. Zero τ_f was achieved for $x \approx 0.625$, at which point in the solid solution $\varepsilon_r \approx 47$. Since both end members have the same tilt system ($a^-a^-c^+$) and space group (*Pnma*), there are no structural phase transitions in the solid solution as a function of composition. Consequently, the plot of ε_r vs τ_f is linear and the mechanism of tuning τ_f may principally be attributed to dilution of the average ionic polarisability, as discussed in detail by Reaney *et al.* [8]. Fig. 12 is a plot of $Q^* f_o$ as a function of x. $Q^* f_o$ is at a maximum (97,000) for the end member LG and decreases to ∼20000 for CT. As expected, $Q^* f_o$ decreases with increasing ε_r, however the presence of second phase in CTLG $x \leq 0.5$ may also contribute to the decrease in the $Q^* f_o$.

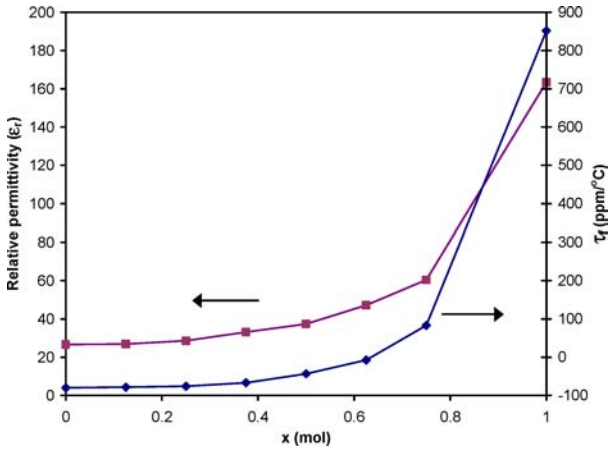

Figure 10 ε_r and τ_f as a function of x for the xCT-$(1-x)$LG ceramics.

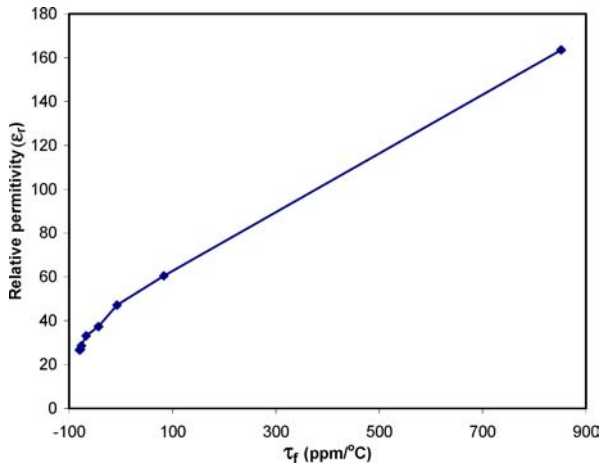

Figure 11 ε_r vs. τ_f for the xCT-$(1-x)$LG ceramics.

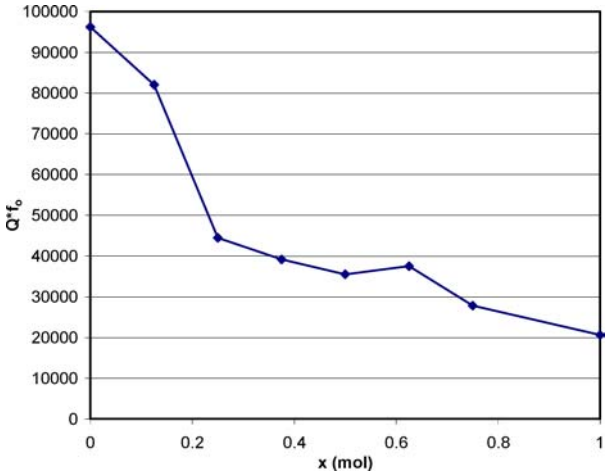

Figure 12 $Q^* f_o$ as a function of x for the xCT-$(1-x)$LG ceramics.

4. Conclusions

In LG, the second phase was confirmed both by EDS and electron diffraction as pyrochlore structured $La_2Zr_2O_7$, which was present due to contamination by the ZrO_2 milling media. In CTLG $x = 0.5$, the second phase was rich in Ca, Ga but deficient in La, Ti and its structure may be indexed according to a body-centred cubic cell ($a \approx 12.5$ Å). It is suggested that the presence of second phase in CTLG series may be in part responsible for the deterioration in $Q^* f_o$ particularly for $x \leq 0.5$. Zero τ_f was achieved at $x \approx 0.65$ at which point in the solid solution $\varepsilon_r \approx 47$ and $Q^* f_o = 40{,}000$, values comparable with commercial systems such as $CaTiO_3$–$NdAlO_3$.

Acknowledgement

This work is sponsored by EPSRC, Filtronic Comtek and Morgan Electroceramics. The authors are very thankful to Mr. R. I. Scott and Mr T. Price at Morgan Electroceramics and Filtronic Comtek respectively for microwave property measurements. The authors would also like to thank Dr. P. Korgul for his assistance with electron microscopy.

References

1. P. L. WISE, I. M. REANEY, W. E. LEE, T. J. PRICE, D. M. IDDLES and D. S. CANNELL, *J. Euro. Ceram. Soc.* **21** (2001) 1723.
2. B. JANCAR, D. SUVOROV and M. VALANT, *J. Mat. Sci. Lett.* **20** (2001) 71.
3. E. A. NENASHEVA, L. P. MUDROLIUBOVA and N. F. KARTENKO, *J. Euro. Ceram. Soc.* **23** (2003) 2443.

4. A. M. GLAZER, *Acta Crystallogr. B* **28** (1972) 3384.
5. C. J. HOWARD and B. J. KENNEDY, *J. Phys.: Cond. Matt.* **11** (1999) 3229.
6. A. M. GLAZER, *Acta Crystallogr. A* **31** (1975) 756.
7. I. M. REANEY, E. L. COLLA and N. SETTER, *Jap. J. Appl. Phys.* **33**(7A) (1994) 3984.
8. P. L. WISE, I. M. REANEY, W. E. LEE, D. M. IDDLES, D. S. CANNEL and T. J. PRICE, *J. Mater. Res.* **17**(8) (2002) 2033.

Received 2 March
and accepted 6 December 2004